

Time correlation functions of three classical Heisenberg spins on an isosceles triangle and on a chain

Marco Ameduri and Richard A. Klemm

Max-Planck-Institut für Physik komplexer Systeme, Nöthnitzer Str. 38, D-01187 Dresden, Germany

(Received 13 August 2001; revised manuscript received 19 September 2002; published 6 December 2002)

At an arbitrary temperature T , we solve for the dynamics of single molecule magnets composed of three classical Heisenberg spins either on a chain with two equal exchange constants J_1 , or on an isosceles triangle with a third, different exchange constant J_2 . As $T \rightarrow \infty$, the Fourier transforms and long-time asymptotic behaviors of the two-spin time correlation functions are evaluated exactly. The lack of translational symmetry on a chain or an isosceles triangle yields time correlation functions that differ strikingly from those on an equilateral triangle with $J_1 = J_2$. At low T , the Fourier transforms of the two autocorrelation functions with $J_1 \neq J_2$ show one and four modes, respectively. For a semi-infinite J_2/J_1 range, one mode is a central peak. At the origin of this range, this mode has an interesting scaling form.

DOI: 10.1103/PhysRevB.66.224404

PACS number(s): 75.10.Hk, 75.75.+a, 75.30.Ds

I. INTRODUCTION

Recently, there has been a substantial interest in the physics of magnetic molecules, or single molecule magnets (SMM's).¹⁻⁷ Such studies are important both for basic scientific reasons and for possible technological applications.^{7,8} Among the smaller SMM's are dimers of V^{4+} ($S = 1/2$) and of Fe^{3+} ($S = 5/2$),^{9,10} a nearly equilateral array of three V^{4+} spins,¹¹ and an isosceles triangle of Gd^{3+} ($S = 7/2$) spins (Gd3).¹² Nonmetallic variations of $9L$ -BaRuO₃ with three Ru^{+4} ($S = 1$) ions (Ru3) might behave as three-spin chain SMM's.^{13,14}

Each SMM consists of a small number of paramagnetic ions surrounded by nonmagnetic chemical ligand groups, and is large enough that the magnetic interactions between the ions in different SMM's within a crystal are negligible. Hence measurements performed on macroscopic samples just probe the magnetic interactions within the individual SMM's. Large single crystals with long-range SMM packing order are suitable for inelastic neutron scattering experiments. Measurements at the appropriate deviations from the Bragg wave vectors for the particular SMM crystal structure probe statistical ensembles of the Fourier transforms of the two-spin time correlation functions involving the spins in each SMM.

The magnetic interactions between the ions in these SMM's can often be described by the isotropic Heisenberg model. One expects that for ions such as Gd^{3+} , with $S = 7/2$, the classical version of the Heisenberg model captures the essential features of the dynamics at not too low temperatures T . For a dimer, comparisons of the classical and $S = 1/2, 5/2$ quantum behaviors of the dynamics supported this expectation.^{15,16} For the equilateral triangle, such comparisons were only made for $T \rightarrow \infty$.¹⁷ In addition, exact and numerical results were presented for the classical dimer,¹⁸⁻²⁰ the four-spin ring,²¹ and the N -spin equivalent neighbor model, which includes the equilateral triangle.²²

For three spins on an equilateral triangle, with equal Heisenberg exchange constants J_1 , the spin sites on each triangle are translationally invariant. Spins on an isosceles

triangle have one additional exchange constant $J_2 \neq J_1$, and this simple translational invariance is absent. Dynamical measurements on Gd3 and modified compositions of Ru3 could help to uncover the effects of this lack of translational invariance inside each SMM, and might aid in our understanding of more complicated systems with multiple magnetic interactions.

At low T , the N spins in the equivalent neighbor model oscillate in a single mode.²² Here we show that the absence of translational symmetry inside each isosceles triangle generally introduces three additional low- T modes at tunable frequencies depending upon $\gamma = J_2/J_1$. For a semi-infinite range of γ values, one of these additional modes is a central peak. In addition, the dynamics of the spins on the endpoints of the three-spin chain with $J_2 = 0$ are qualitatively different from the dynamics of the spin at the chain center. The mode tuning parameter γ makes the dynamical behavior of the spins on an isosceles triangle remarkably different from that present in any SMM system studied previously, including the four-spin ring.^{21,22}

The structure of the paper is as follows: In Sec. II we define the model, calculate its partition function, and present the exact time evolution of the spin vectors. In Secs. III and IV, we discuss the time dependence and Fourier transform, respectively, of each spin-spin correlation function. We discuss our results in Sec. V.

II. MODEL AND SPIN DYNAMICS

We study the Hamiltonian describing three spins S_i of unit magnitude, $S_i = |S_i| = 1$, on a triangle with two classical Heisenberg exchange couplings,

$$H = -J_1(\mathbf{S}_1 \cdot \mathbf{S}_2 + \mathbf{S}_2 \cdot \mathbf{S}_3) - J_2 \mathbf{S}_1 \cdot \mathbf{S}_3. \quad (1)$$

The cases $J_1 = J_2$ and $J_1 \neq J_2 \neq 0$ describe equilateral and isosceles triangles, respectively. The case $J_2 = 0$ describes a three-spin chain with free boundary conditions. Equation (1) can be realized if the ring contains either two different lattice constants, as in Gd3, or ions with two different spin values.

We rewrite Eq. (1) in terms of the total spin $\mathbf{S}=\mathbf{S}_2+\mathbf{S}_{13}$, with $\mathbf{S}_{13}=\mathbf{S}_1+\mathbf{S}_3$, and obtain, up to a constant,

$$H=-\frac{J_1}{2}\mathbf{S}^2-\frac{J_2-J_1}{2}\mathbf{S}_{13}^2. \quad (2)$$

The partition function $Z=\int(\prod_{i=1}^3d\Omega_i/4\pi)e^{-\beta H}$ is

$$Z=\int_0^2dx\int_{|x-1|}^{x+1}dsse^{-\beta H}=\frac{e^\alpha}{\alpha}\int_0^2dxe^{\alpha\gamma x^2}\sinh(2\alpha x), \quad (3)$$

where $\beta=(k_B T)^{-1}$, $d\Omega_i$ is the solid angle element for the i th spin, $\alpha=\beta J_1/2$, $\gamma=J_2/J_1$, $x=S_{13}$, and $s=S$.

To calculate the time-dependent correlation functions $\langle\mathbf{S}_i(t)\cdot\mathbf{S}_j(0)\rangle$, we first solve the classical Heisenberg equations of motion for the quantities $\mathbf{S}_2(t)$ and $\mathbf{S}_{13}(t)$,

$$\dot{\mathbf{S}}_{2,13}=J_1\mathbf{S}_{2,13}\times\mathbf{S}, \quad (4)$$

leading to

$$\mathbf{S}_{2,13}(t)=C_{2,13}\hat{\mathbf{s}}+A_{2,13}[\cos(J_1st)\hat{\mathbf{x}}-\sin(J_1st)\hat{\mathbf{y}}], \quad (5)$$

where $\hat{\mathbf{s}}\|\mathbf{S}$, $\hat{\mathbf{s}}=\hat{\mathbf{x}}\times\hat{\mathbf{y}}$, $A_2=-A_{13}$, $C_2+C_{13}=s$, $C_{13}=(s^2+x^2-1)/(2s)$, and $A_{13}^2=x^2-C_{13}^2$.

The time dependence of \mathbf{S}_1 (or \mathbf{S}_3) is obtained from

$$\dot{\mathbf{S}}_1=(J_2-J_1)\mathbf{S}_1\times\mathbf{S}_{13}+J_1\mathbf{S}_1\times\mathbf{S}, \quad (6)$$

leading to

$$S_{1s}(t)=S_{1s0}+\Delta S_{1s0}\cos[(J_1-J_2)xt-\phi_0], \quad (7)$$

$$\begin{aligned} S_{1\pm}(t) &= \frac{A_{13}S_{1s0}}{C_{13}}\exp(\mp isJ_1t) + \frac{A_{13}\Delta S_{1s0}}{2(C_{13}+x)}\exp\left\{\mp i[(J_1s \right. \\ &+ (J_1-J_2)x]t \pm i\phi_0\} + \frac{A_{13}\Delta S_{1s0}}{2(C_{13}-x)}\exp\{\mp i[(J_1s \\ &- (J_1-J_2)x]t \mp i\phi_0\}, \quad (8) \end{aligned}$$

where $S_{1\pm}=S_{1x}\pm iS_{1y}$, $S_{1s0}=C_{13}/2$, $\Delta S_{1s0}=A_{13}(1-x^2/4)^{1/2}/x$, and ϕ_0 is an arbitrary angle describing the initial spin configuration.²¹

III. TIME CORRELATION FUNCTIONS

We study the two-spin time correlation functions

$$C_{ij}(t)=\langle\mathbf{S}_i(t)\cdot\mathbf{S}_j(0)\rangle, \quad (9)$$

where $\langle\cdots\rangle=\int_0^2d\phi_0\int_0^2dx\int_{|x-1|}^{x+1}dsse^{-\beta H}\cdots/(2\pi Z)$. Since $C_{11}=C_{33}$ and $C_{12}=C_{23}$, only four C_{ij} are independent. These are constrained by the sum rule

$$\langle s^2\rangle=C_{22}(t)+2C_{11}(t)+4C_{12}(t)+2C_{13}(t). \quad (10)$$

After averaging over ϕ_0 , the exact $C_{ij}(t)$ satisfy

$$C_{11}(t)=I_0+I_1(t)+I_2(t)+I_3(t), \quad (11)$$

$$C_{13}(t)=I_0+I_1(t)-I_2(t)-I_3(t), \quad (12)$$

$$C_{22}(t)=4[I_0+I_1(t)]+2\langle C_2s\rangle-\langle s^2\rangle, \quad (13)$$

$$C_{12}(t)=-2[I_0+I_1(t)]+\frac{1}{2}[\langle s^2\rangle-\langle C_2s\rangle], \quad (14)$$

where, by setting $t^*=J_1t$, we have

$$I_0=\frac{1}{4}\langle C_{13}^2\rangle, \quad (15)$$

$$I_1(t)=\frac{1}{4}\langle A_{13}^2\cos(st^*)\rangle, \quad (16)$$

$$I_2(t)=\frac{1}{2}\left\langle\frac{A_{13}^2}{x^2}\left(1-\frac{x^2}{4}\right)\cos[(1-\gamma)xt^*]\right\rangle, \quad (17)$$

$$\begin{aligned} I_3(t) &= \left\langle\frac{(1-x^2/4)}{4x^2}((C_{13}-x)^2\cos\{[s+(1-\gamma)x]t^*\} \right. \\ &+ (C_{13}+x)^2\cos\{[s-(1-\gamma)x]t^*\})\left.\right\rangle. \quad (18) \end{aligned}$$

As $T\rightarrow\infty$, the remaining double integrals in Eqs. (15)–(18) can be reduced to single integrals, as shown in the Appendix. Note that $I_2(t)$ is a constant for $\gamma=1$, but not for $\gamma\neq 1$, leading to dramatic differences between the dynamics of spins on equilateral and isosceles triangles, respectively. As $t\rightarrow\infty$, the time-dependent integrands oscillate wildly and their contributions vanish.²³ From Eqs. (13) and (16), $\lim_{T,t\rightarrow\infty}C_{22}$ for $\gamma\neq 1$ is identical to its value for $\gamma=1$. Only at finite T does J_2 influence $C_{22}(t)$. Hence, for $t^*\gg 1$ and $T\rightarrow\infty$,^{21,24}

$$\lim_{\substack{T\rightarrow\infty \\ t^*\gg 1}}C_{22}(t)\sim\frac{1}{3}+2\delta_3-\frac{\sin(t^*)+\sin(3t^*)}{(t^*)^3}, \quad (19)$$

$$\delta_3=\frac{9}{80}\ln 3-\frac{1}{20}\approx 0.07359. \quad (20)$$

From Eqs. (13) and (14), it then follows that

$$\lim_{\substack{T\rightarrow\infty \\ t^*\gg 1}}C_{12}(t)\sim\frac{1}{3}-\delta_3+\frac{\sin(t^*)+\sin(3t^*)}{2(t^*)^3}. \quad (21)$$

The surprise comes from the behaviors of C_{11} and C_{13} . The long-time approaches to the various asymptotic limits are characterized by three different powers, corresponding to the equilateral, the isosceles, and the chain cases, respectively. For $\gamma=1$, $C_{11}^{\gamma=1}(t)=C_{22}(t)$, which approach their mutual limit as t^{-3} as $T\rightarrow\infty$.

For $\gamma=0$, $C_{11}(t)$ is dominated by $I_3(t)$, yielding

$$\lim_{\substack{T\rightarrow\infty \\ t^*\gg 1}}C_{11}^{\gamma=0}(t)\sim\frac{1}{3}+\frac{\delta_3}{2}+\frac{1}{2t^*}\sin(t^*), \quad (22)$$

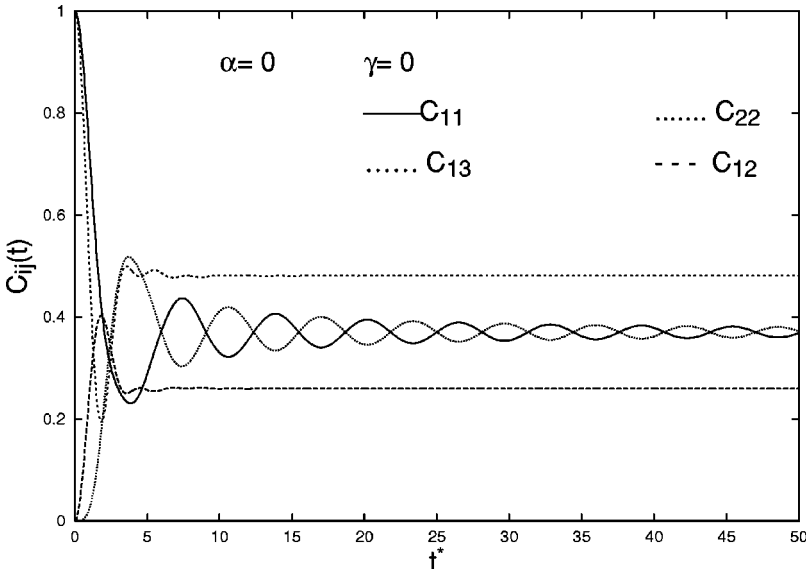


FIG. 1. Plots of $C_{11}(t)$ (solid), $C_{12}(t)$ (dashed), $C_{13}(t)$ (dense dotted, $C_{13}(0)=0$), $C_{22}(t)$ (sparse dotted, $C_{22}(0)=1$) vs $t^*=|J_1|t$ as $T \rightarrow \infty$ ($\alpha=0$) for the chain ($\gamma=0$).

which approaches its different asymptotic limit dramatically slower.

For $\gamma \neq 0, 1$, $I_2(t)$ and $I_3(t)$ decay as t^{-2} and oscillate with different frequencies. The evaluation of $I_3(t)$ is quite involved. By calculating its Fourier transform and then inverting it through integration by parts, we find

$$\lim_{T \rightarrow \infty} \frac{C_{11}^{\gamma \neq 0, 1}(t)}{|\gamma|t^*, |1-\gamma|t^* \gg 1} \sim \frac{1}{3} + \frac{\delta_3}{2} + \frac{\{a_1 + a_2 \cos[2(1-\gamma)t^*] + a_3 \cos(t^*)\}}{(t^*)^2}, \quad (23)$$

where (see the Appendix)

$$a_1 = -\frac{1}{6(1-\gamma)^2}, \quad (24)$$

$$a_2 = -\frac{1}{(1-\gamma)^2} \left(\frac{5}{32} - \frac{9}{128} \ln 3 \right) \approx -\frac{0.079004}{(1-\gamma)^2}, \quad (25)$$

$$a_3 = -\frac{\gamma-1}{2\gamma} + \frac{\gamma-2}{4} \ln \left| \frac{\gamma}{\gamma-2} \right|. \quad (26)$$

Note that one cannot take either of the limits $\gamma \rightarrow 1$ or $\gamma \rightarrow 0$ directly in Eq. (23), since the expansion is valid only when both $|\gamma|t^* \gg 1$ and $|1-\gamma|t^* \gg 1$ are satisfied.

In Fig. 1, we plot the $C_{ij}(t)$ as $T \rightarrow \infty$ for $\gamma=0$. Since $C_{22}(t)$ and $C_{12}(t)$ as $T \rightarrow \infty$ are independent of γ , these curves are respectively identical to those for $C_{11}(t)$ and $C_{12}(t)$ obtained for $T \rightarrow \infty$ in the equilateral triangle. These functions each approach their asymptotic limits as t^{-3} . On the other hand, for $\gamma=0$, $C_{11}(t)$ and $C_{13}(t)$ oscillate about each other for a long time, approaching their mutual asymptotic limit as t^{-1} .

In Fig. 2 we compare $C_{11}(t)$ and $C_{13}(t)$ as $T \rightarrow \infty$ for γ

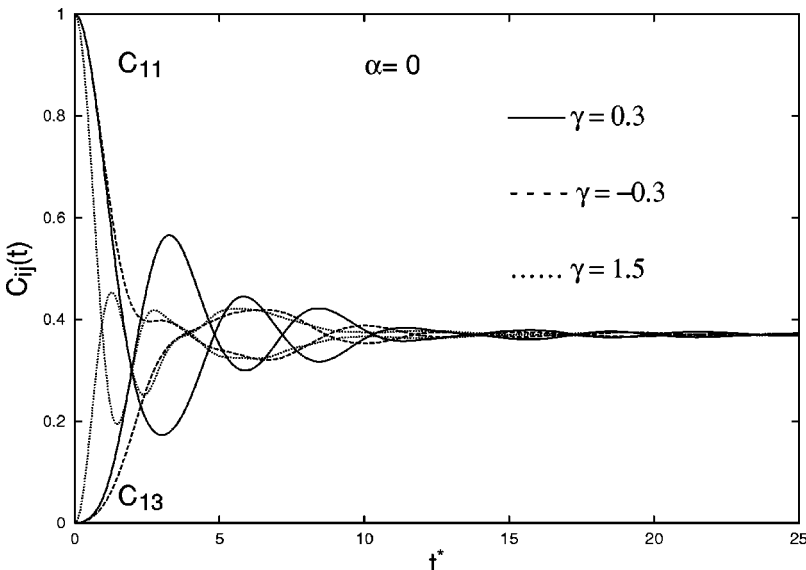


FIG. 2. Plots of $C_{11}(t)$, $C_{13}(t)$ vs $t^*=|J_1|t$ for $T \rightarrow \infty$ ($\alpha=0$), $\gamma=0.3$ (solid), -0.3 (dashed), and 1.5 (dotted).

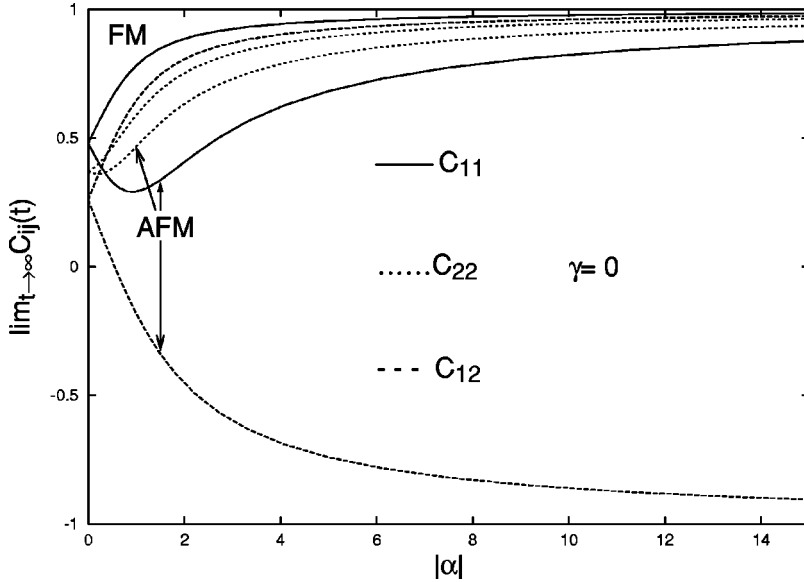


FIG. 3. Plots of $\lim_{t \rightarrow \infty} C_{ij}(t)$ for the chain ($\gamma=0$) vs $|\alpha| = \beta|J_1|/2$, for $\alpha > 0$ (FM) and $\alpha < 0$ (AFM).

$= \pm 0.3$ and 1.5 . For $\gamma = \pm 0.3$, the leading term in the approach to the asymptotic limit arises from a_3 in Eq. (23). For $\gamma = 1.5$, $2|1 - \gamma| = 1$, so there is asymptotically only one frequency, equal to that for the chain shown in Fig. 1, but the asymptotic limit is approached faster.

At finite T , the physics of the model is influenced not only by γ , but also by the sign of J_1 . We henceforth refer to the $J_1 > 0$ and $J_1 < 0$ cases as ferromagnetic (FM) and antiferromagnetic (AFM), respectively.

We obtain the $C_{ij}(t)$ at finite T by direct numerical evaluation of the double integrals in Eqs. (11)–(14). As an example, in Fig. 3, we plot the $\lim_{t \rightarrow \infty} C_{ij}(t)$ for $\gamma = 0$ as functions of $|\alpha| = \beta|J_1|/2$. The FM and AFM cases are distinguished by arrows. We recall that $\lim_{t \rightarrow \infty} C_{13}(t) = \lim_{t \rightarrow \infty} C_{11}(t)$ for all $\gamma \neq 1$. The spins are intrinsically unfrustrated. At low T , the FM $\lim_{t \rightarrow \infty} C_{ij}(t) \sim 1$, while the AFM $\lim_{t \rightarrow \infty} C_{12}(t) \sim -1$. In the AFM case, $\lim_{t \rightarrow \infty} C_{11}(t)$ has a minimum value of ~ 0.29 at $\alpha \sim -0.9$.

IV. FOURIER TRANSFORMS

The dimensionless Fourier transform (FT) of each deviation $\delta C_{ij}(t) \equiv C_{ij}(t) - \lim_{t \rightarrow \infty} C_{ij}(t)$,²¹ is

$$\delta \tilde{C}_{ij}(\omega) = \frac{|J_1|}{\pi} \int_{-\infty}^{+\infty} dt e^{i\omega t} \delta C_{ij}(t). \quad (27)$$

Since causality requires $\delta \tilde{C}_{ij}(\omega) = \delta \tilde{C}_{ij}(-\omega)$, we consider only positive values of ω/J_1 . The Fourier integral is in principle elementary, since the time dependence is contained in simple trigonometric factors, yielding combinations of δ functions that allow us to perform one of the integrations. We thus obtain single integral representations for the FT's at any T , which can be evaluated with high precision. Since each integration domain is restricted to a finite region in the (s, x) plane, the δ -functions only contribute to the integrals if ω falls within specific ranges. Determining the allowed ranges of ω values is tedious. Some of the details of this calculation are presented in the Appendix.

A. Infinite temperature

In Fig. 4 we plot $\delta \tilde{C}_{11}(\omega)$ as $T \rightarrow \infty$ for some $|\gamma| \leq 1$. The solid curves for $\gamma = 1, 0$ correspond to the equilateral triangle and the chain. For the equilateral triangle, $\delta \tilde{C}_{11}(\omega)$ vanishes as $\omega \rightarrow 0, 3$, and exhibits a single smooth peak at $\omega/|J_1| \approx 1.4385$. Although difficult to discern in this figure, the curve contains discontinuous second derivatives at $\omega/|J_1| = 1, 3$ responsible for the t^{-3} long-time, $T \rightarrow \infty$ decay of $\delta C_{11}(t)$.^{21,22}

As $T \rightarrow \infty$, although $\delta \tilde{C}_{22}(\omega)$ for the chain coincides with the equilateral triangle $\delta \tilde{C}_{11}(\omega)$ curve, the chain $\delta \tilde{C}_{11}(\omega)$ is dramatically different. In addition to the slope discontinuity at $\omega/|J_1| = 2$, the chain $\delta \tilde{C}_{11}(\omega)$ is discontinuous at $\omega/|J_1| = 1$, as indicated by the symbol \approx . This discontinuity is responsible for the $1/t$ long-time, $T \rightarrow \infty$ decay of $\delta C_{11}(t)$.

The isosceles triangle cases are also very interesting, as they do not just interpolate between the equilateral triangle and the chain. For $\gamma = \pm 0.2$, the discontinuities in the slope of $\delta \tilde{C}_{11}(\omega)$ at $\omega/|J_1| = 1, 1.4$, and 1.6 are also discernible. As $\gamma \rightarrow 0$, the slope discontinuities at $\omega/|J_1| = 1$ approach $\pm \infty$ as expressed in Eq. (26). In addition, there is a large discontinuity in the slope of the curve for $\gamma = 0.9$ at $\omega/|J_1| = 0.2$, and a resulting large peak at $\omega/|J_1| \approx 0.088$, arising from $\tilde{T}_2(\omega)$. This slope discontinuity is responsible for the first two terms $\propto t^{-2}$ in Eq. (23).

B. Low temperature

The $\delta \tilde{C}_{ij}(\omega)$ at finite T were obtained by numerical evaluation of the single integrals defined in the Appendix. As $T \rightarrow \infty$, we compared our numerical and analytic results. At finite T we also checked the initial value sum rules by integrating the FT's in Eq. (27).

1. Equilateral triangle

We first discuss the equilateral triangle, $\gamma = 1$. For the AFM case, As T decreases, the single peak in $\delta \tilde{C}_{11}(\omega)$ grows

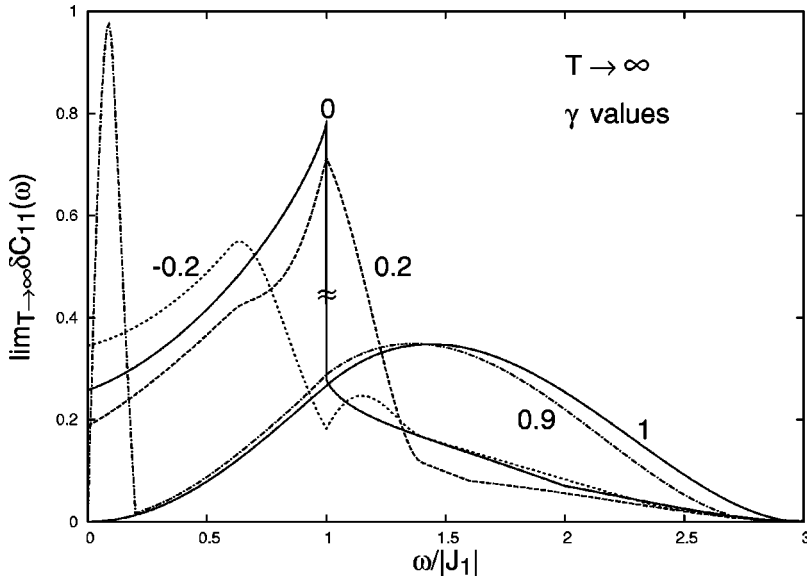


FIG. 4. Plots of $\delta \tilde{C}_{11}(\omega)$ as functions of $\omega/|J_1|$ as $T \rightarrow \infty$, for $\gamma = 1, 0$ (solid), 0.2 (dashed), -0.2 (dotted), and 0.9 (dash dotted).

in amplitude and shifts to lower $\omega/|J_1|$. As shown for the equivalent neighbor model,²² this behavior can be quantified by plotting $|\alpha|^{-1/2} \delta \tilde{C}_{11}(\omega)$ versus $\tilde{\omega} = |\alpha|^{1/2} \omega/|J_1|$. In Fig. 5, the $|\alpha|^{-1/2} \delta \tilde{C}_{11}(\omega)$ curves approach the uniform AFM equivalent neighbor model form $(8/3\sqrt{\pi}) \tilde{\omega}^2 \exp(-\tilde{\omega}^2)$, shown as the solid curve, as $T \rightarrow 0$.²² This frustrated behavior results in a scaling of the time, as $\mathcal{C}(t)$ approaches a uniform function of $(JT)^{1/2} t$ as $T \rightarrow 0$.

For the FM equilateral triangle, as T decreases, the peak in $\delta \tilde{C}_{11}(\omega)$ shifts asymptotically to $3J_1$, as all of the spins oscillate together. In the equivalent neighbor model, as $T \rightarrow 0$, the three-spin $\gamma = 1$ FM curves approach a uniform function of $(\omega/J_1 - \omega_3^*) \alpha$, where $\omega_3^* = 3 - 1/(3|\alpha|)$, as shown in Fig. 6.²² That is, as $T \rightarrow 0$, the peak amplitude tends to a constant value, but its maximum position approaches $3J_1$ linearly in T .

2. Three-spin chain

A strikingly different behavior is obtained for the low- T AFM chain. In this case, instead of the single AFM mode present in the equilateral triangle, there are *four* modes, the frequencies Ω_i of which approach $\Omega_i/|J_1| = 1, 2,$ and 3 as $T \rightarrow 0$ as the frequencies of the strongest modes Ω_1 and Ω_2 , become degenerate. In Fig. 7, we plotted $\delta \tilde{C}_{11}(\omega)$ and $\delta \tilde{C}_{22}(\omega)$ for these two modes, versus $(\omega/|J_1| - 1)2|\alpha|/5$, at various low- T α values. Curves for $\delta \tilde{C}_{22}(\omega)$ are shifted to the right by 0.2 for clarity. We note that $\delta \tilde{C}_{11}(\omega)$ for the Ω_2 mode has a shallow maximum at a frequency which approaches $|J_1|$ from above as $T \rightarrow 0$. For the Ω_1 mode, $\delta \tilde{C}_{11}$ has a large discontinuity precisely at $\omega/|J_1| = 1$ for all T . By contrast, the $\delta \tilde{C}_{22}(\omega)$ curves only exhibit the Ω_2 mode, and are smooth and rather symmetric about their maxima. Both

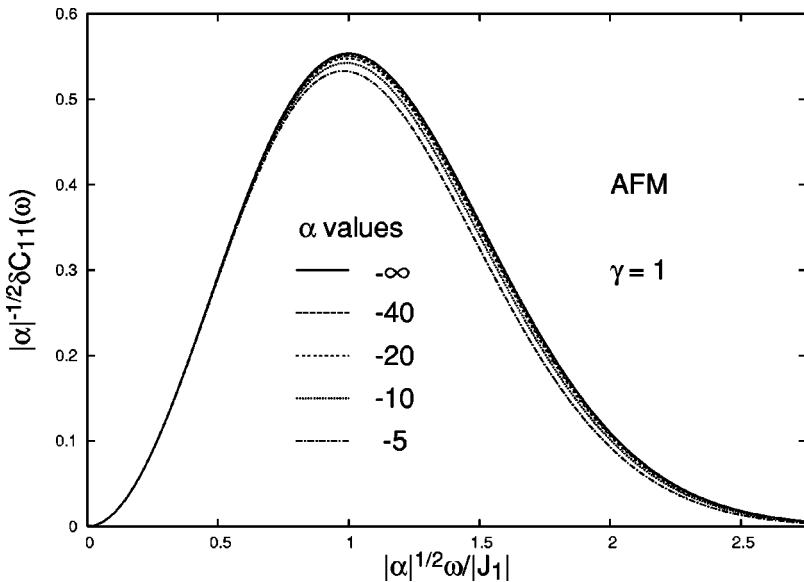


FIG. 5. Plots of $|\alpha|^{-1/2} \delta \tilde{C}_{11}(\omega)$ vs $|\alpha|^{1/2} \omega/|J_1|$ for the AFM equilateral triangle at low T .

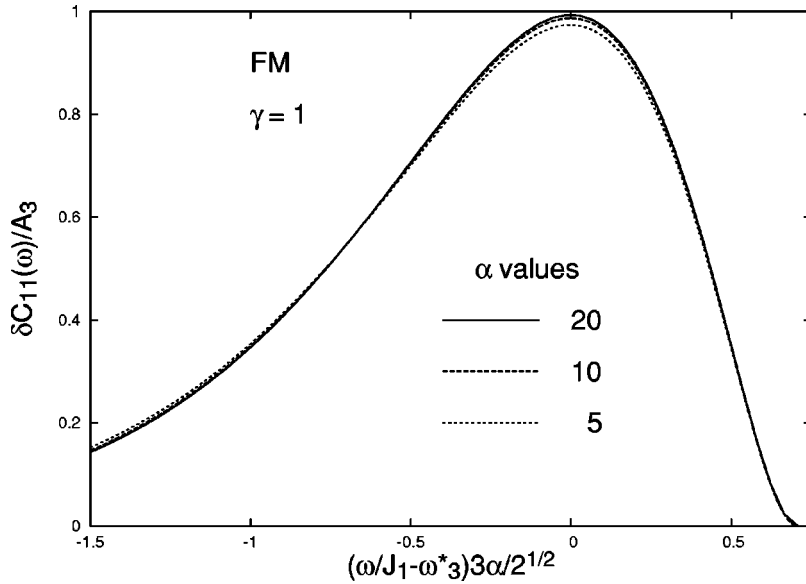


FIG. 6. Plots of $\delta\tilde{C}_{11}(\omega)/A_3$ vs $(\omega/J_1 - \omega_3^*)3\alpha/2^{1/2}$ for the FM equilateral triangle at low T , where $A_3=8/(3e^2)$ and $\omega_3^*=3 - 1/(3|\alpha|)$.

$\delta\tilde{C}_{ii}(\omega)$ for these modes approach a uniform scaling function of $|\alpha|(\omega/|J_1| - 1)$ as $T \rightarrow 0$. We remark that the low- T scaling behaviors of the dominant modes in the AFM chain are similar to that of the FM equilateral triangle, since neither of these mode energies approaches 0 as $T \rightarrow 0$.

In addition, we found that the weaker Ω_3 and Ω_4 modes, for which $\delta\tilde{C}_{11}(\omega)$ is peaked at $\omega/|J_1| \approx 3, 2$, respectively, both approach uniform low- T scaling functions. For the Ω_3 mode, $|\alpha|\delta\tilde{C}_{11}(\omega)$ approaches a uniform scaling function of $|\alpha|(\omega/|J_1| - 3)$, and for the Ω_4 mode, $\alpha^2\delta\tilde{C}_{11}(\omega)$ approaches a uniform scaling function of $|\alpha|(\omega/|J_1| - 2)$ as $T \rightarrow 0$. Hence, as $T \rightarrow 0$, the amplitudes of these modes vanish as T and T^2 , respectively.

For the FM chain at low T , there are four nondegenerate modes for which $\delta\tilde{C}_{11}(\omega)$ is peaked at $\Omega_i/|J_1| \approx 1, 2, 3$, and 5. At low T , the two largest intensity modes Ω_2 and Ω_1 , which are peaked at $\omega/|J_1| \approx 1, 3$, respectively, are pictured for $\alpha=5, 10$, and 20 in Fig. 8. At low T , $\delta\tilde{C}_{11}$ for the Ω_2 mode

is very large for $\omega/|J_1| < 1$, but drops *discontinuously to zero* at $\omega/|J_1| = 1$, as shown in Fig. 8. For the next largest intensity mode, Ω_1 , both $\delta\tilde{C}_{11}(\omega)$ and the larger $\delta\tilde{C}_{22}(\omega)$ exhibit peak positions that approach $\omega/|J_1| = 3$ as $T \rightarrow 0$, as shown in Fig. 8. We note that we have multiplied the intensities of these curves by a factor of 9, and squeezed the scaling variable by a factor of 3, relative to those of $\delta\tilde{C}_{11}$ for the Ω_2 mode, in order to fit all three sets of curves in the same figure. All of the curves shown in Fig. 8 scale as for the FM equilateral triangle. As for the AFM chain, at low T , $\alpha\delta\tilde{C}_{11}(\omega)$ for the Ω_4 mode approaches a uniform function of $(\omega/|J_1| - 2)|\alpha|$, and $\alpha^2\delta\tilde{C}_{11}(\omega)$ for the weakest mode Ω_3 approaches a uniform function of $(\omega/|J_1| - 5)|\alpha|$.

3. General isosceles triangle

We now consider the more general isosceles triangle cases. We first discuss the AFM cases $J_1 < 0$. As for the chain, for $\gamma \neq 1$, as T is lowered, $\delta\tilde{C}_{11}(\omega)$ generally develops

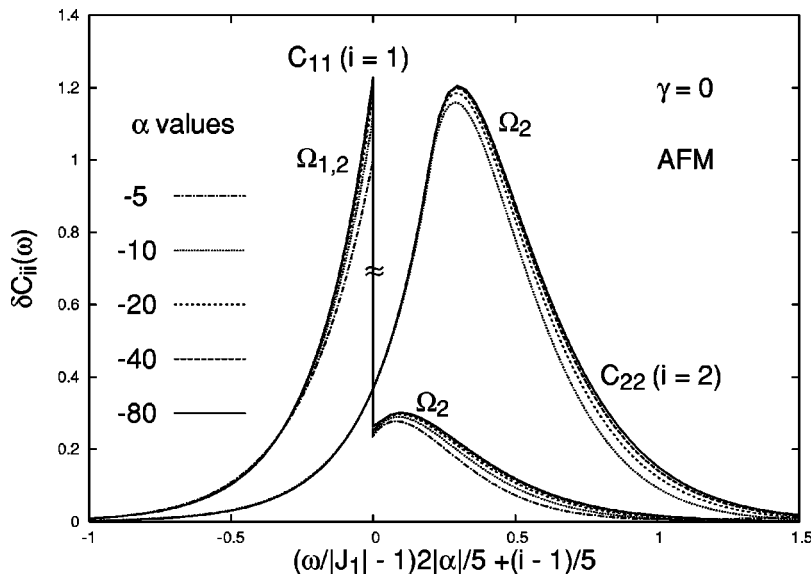


FIG. 7. Plots of $\delta\tilde{C}_{11}(\omega)$ vs $(\omega/|J_1| - 1)2|\alpha|/5$ and $\delta\tilde{C}_{22}(\omega)$ vs $(\omega/|J_1| - 1)2|\alpha|/5 + 0.2$, for the AFM chain at the low- T values $-\alpha=5, 10, 20, 40$, and 80. $\tilde{C}_{11}(\omega)$ is discontinuous at $\omega/|J_1|=1$, indicated by the \approx .

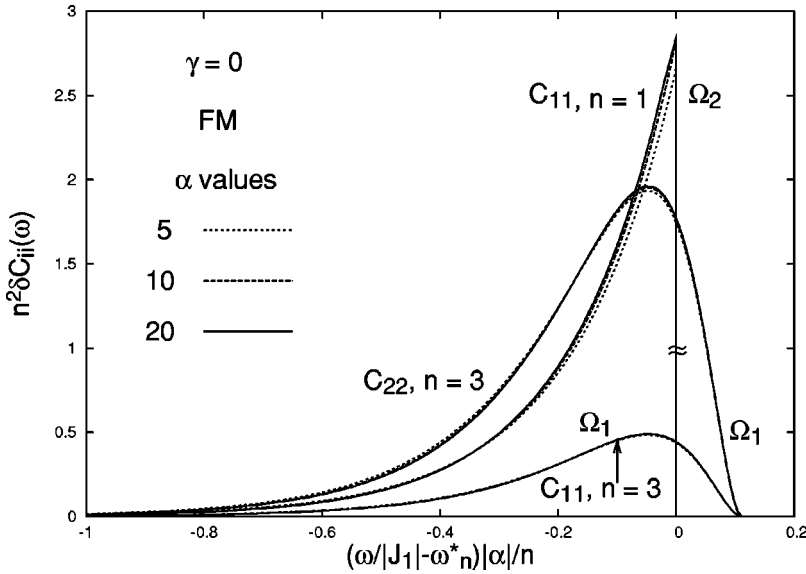


FIG. 8. Plots of $n^2 \delta \tilde{C}_{11}(\omega)$ and $n^2 \delta \tilde{C}_{22}(\omega)$ vs $(\omega/|J_1| - \omega_n^*)|\alpha|/n$ for the Ω_1 and Ω_2 modes of the FM chain at the low- T values $\alpha=5, 10$, and 20 , where $\omega_n^* = n - (n-1)/(2n|\alpha|)$. $\tilde{C}_{11}(\omega)$ for the Ω_2 mode is discontinuous at $\omega/|J_1|=1$, as indicated by the \approx .

into three or four peaks, which become progressively sharper. When only three modes are present, one of them is a central peak at $\omega=0$. For nonvanishing frequencies, these modes are magnons. As for the three-spin chain, their relative intensities at finite T are very different, as the two largest are typically a few orders of magnitude larger than the third, which is a few orders of magnitude larger than the fourth.

To illustrate the types of low- T AFM behavior, in Fig. 9 we plot $\log_{10}[\delta \tilde{C}_{11}(\omega)]$ and $\log_{10}[\delta \tilde{C}_{22}(\omega)]$ versus $\omega/|J_1|$ at the AFM low- T value $\alpha=-80$ for $\gamma=-0.1$ and 2.5 . For $\gamma=-0.1$, $\delta \tilde{C}_{11}(\omega)$ exhibits four sharp peaks at $\omega/|J_1| \approx 1, 1.2, 2.2$, and 3.2 . For $\gamma=2.5$, there are three broad peaks in $\delta \tilde{C}_{11}(\omega)$, one of which is a central peak at $\omega=0$, and the others are centered at $\omega/|J_1| \approx 0.6$ and 1.2 . In each case, $\delta \tilde{C}_{22}(\omega)$ is a single peak at one of the larger nonvanishing $\delta \tilde{C}_{11}(\omega)$ peak positions.

After a careful analysis of many lower- T results, we established simple formulas relating the frequencies of the

modes to γ . $\delta \tilde{C}_{11}(\omega)$ contains four low- T AFM mode frequencies, $\Omega_i(\gamma)$, depicted in Fig. 10, which satisfy

$$\begin{aligned} \Omega_1(\gamma)/|J_1| &= 1 \quad \text{for } \gamma \leq 1/2, \\ &= |1 - 1/\gamma| \quad \text{for } \gamma \geq 1/2, \end{aligned} \quad (28)$$

$$\begin{aligned} \Omega_2(\gamma)/|J_1| &= 1 - 2\gamma \quad \text{for } \gamma \leq 1/2, \\ &= 0, \quad \text{for } \gamma \geq 1/2, \end{aligned} \quad (29)$$

$$\begin{aligned} \Omega_3(\gamma)/|J_1| &= 3 - 2\gamma \quad \text{for } \gamma \leq 1/2, \\ &= 2|1 - 1/\gamma| \quad \text{for } \gamma > 1/2, \end{aligned} \quad (30)$$

$$\begin{aligned} \Omega_4(\gamma)/|J_1| &= 2 - 2\gamma \quad \text{for } \gamma \leq 1/2, \\ &= |1 - 1/\gamma| \quad \text{for } \gamma \geq 1/2. \end{aligned} \quad (31)$$

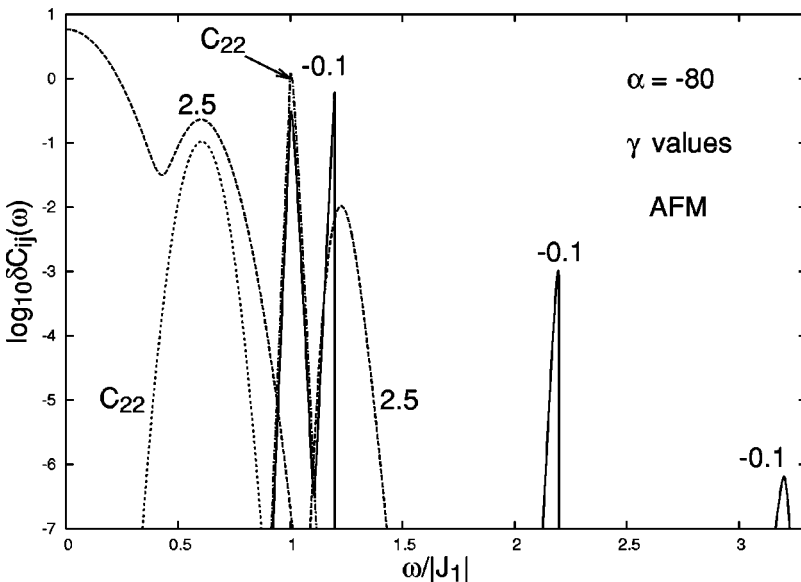


FIG. 9. Plots of the AFM $\log_{10}[\delta \tilde{C}_{ij}(\omega)]$ vs $\omega/|J_1|$, at low T ($\alpha=-80$) for $\gamma=-0.1, 2.5$. The solid (dashed) curves correspond to $\delta \tilde{C}_{11}(\omega)$ for $\gamma=-0.1$ (2.5). The dash-dotted (dotted) curves are the corresponding $\delta \tilde{C}_{22}(\omega)$ curves.

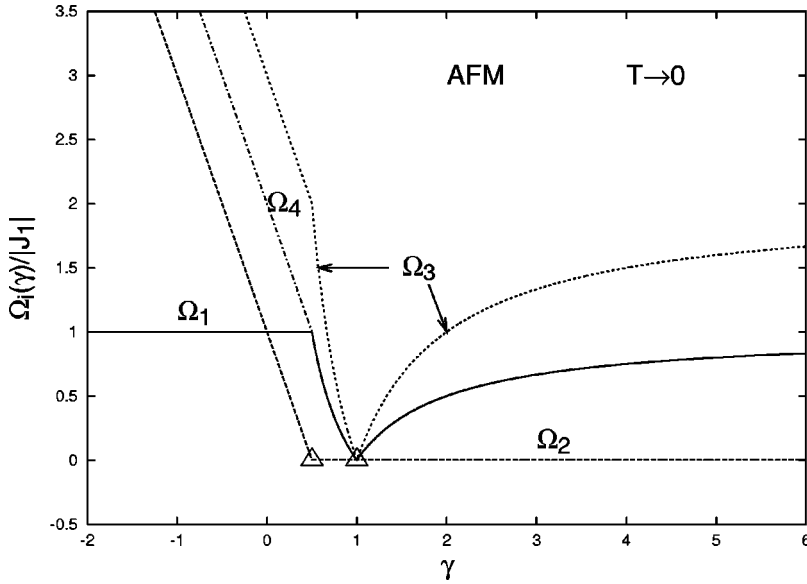


FIG. 10. Plots of the low- T AFM mode frequencies $\Omega_i(\gamma)/|J_1|$ vs γ . The triangles indicate low- T scaling.

$\delta\tilde{C}_{22}(\omega)$ contains only the low- T FM mode with frequency $\Omega_1(\gamma)$. We note that for $\gamma \geq 1/2$, Ω_4 and Ω_1 are degenerate. We analytically confirmed Eq. (28) by performing an asymptotic evaluation of the integral representation of $\delta\tilde{C}_{22}(\omega)$, as shown in the Appendix.

For the AFM case with $\gamma < 1/2$, there are four modes at finite frequencies. For $1 \neq \gamma > 1/2$, Ω_1 and Ω_4 are degenerate, and the mode with frequency $\Omega_2(\gamma) = 0$ is a central peak. The two triangles in Fig. 10 indicate special points. For $\gamma = 1$, the four modes are all degenerate, $\delta\tilde{C}_{11}(\omega) = \delta\tilde{C}_{22}(\omega)$, and $\delta\tilde{C}_{11}(\omega)$ approaches the AFM scaling form shown in Fig. 5. For the low- T AFM case $\gamma = 1/2$, $\delta\tilde{C}_{11}(\omega)$ exhibits the mode frequency $\Omega_2(1/2) \rightarrow |J_2|/|\alpha|^{1/2}$ as $T \rightarrow 0$, and the shape of this mode approaches a scaling function of $|\alpha|^{1/2}\omega/|J_1|$, as shown in Fig. 11. These $\delta\tilde{C}_{11}(\omega)$ curves scale *without* a corresponding rescaling of $\delta\tilde{C}_{11}(\omega)$ itself.

We now consider the FM case at low T . To illustrate the types of behavior found, in Fig. 12, we plot $\log_{10}[\delta\tilde{C}_{11}(\omega)]$

and $\log_{10}[\delta\tilde{C}_{22}(\omega)]$ versus $\omega/|J_1|$ at $\alpha = 20$ for $\gamma = 1.5$ and -1 . For $\gamma = 1.5$, $\delta\tilde{C}_{11}(\omega)$ at this T exhibits four sharp modes at $\omega/|J_1| \approx 1, 2, 3$, and 4 , respectively. For $\gamma = -1$, there are three broad $\delta\tilde{C}_{11}(\omega)$ modes, with rather well-defined peaks at $\omega/|J_1| \approx 0, 2, 3.6$ at this T . As for the AFM case, in each case $\delta\tilde{C}_{22}(\omega)$ is a single peak at one of the nonvanishing $\delta\tilde{C}_{11}(\omega)$ peak positions.

From an extensive analysis of many lower- T results, we found that there are generally four low- T $\delta\tilde{C}_{11}(\omega)$ FM mode frequencies, $\Omega_i(\gamma)$, and that $\delta\tilde{C}_{22}(\omega)$ has one nonvanishing mode frequency $\Omega_1(\gamma)$. These FM $\Omega_i(\gamma)$, pictured in Fig. 13, satisfy

$$\begin{aligned} \Omega_1(\gamma)/J_1 &= |1 - 1/\gamma| \quad \text{for } \gamma \leq -1/2, \\ &= 3 \quad \text{for } \gamma \geq -1/2, \end{aligned} \tag{32}$$

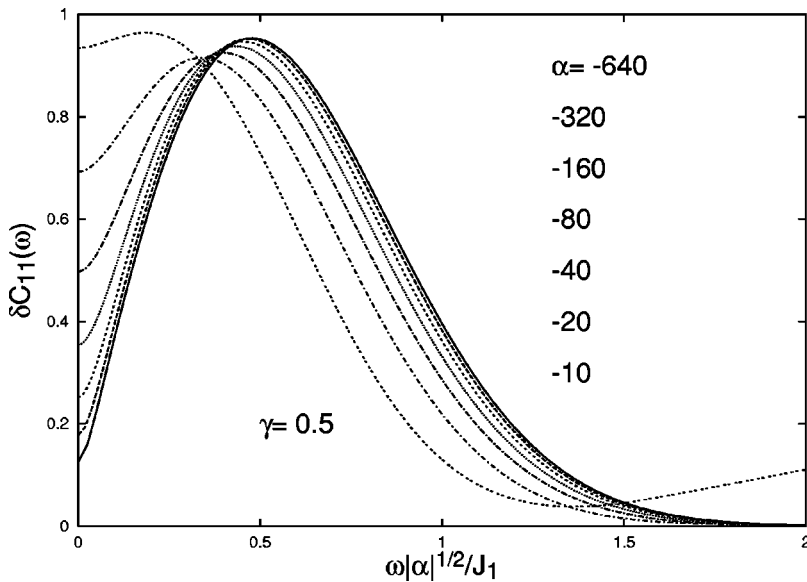


FIG. 11. Low- T plots of $\delta\tilde{C}_{11}(\omega)$ vs the scaled frequency $\omega|\alpha|^{1/2}/|J_1|$ displaying the AFM $\Omega_2(1/2)$ mode.

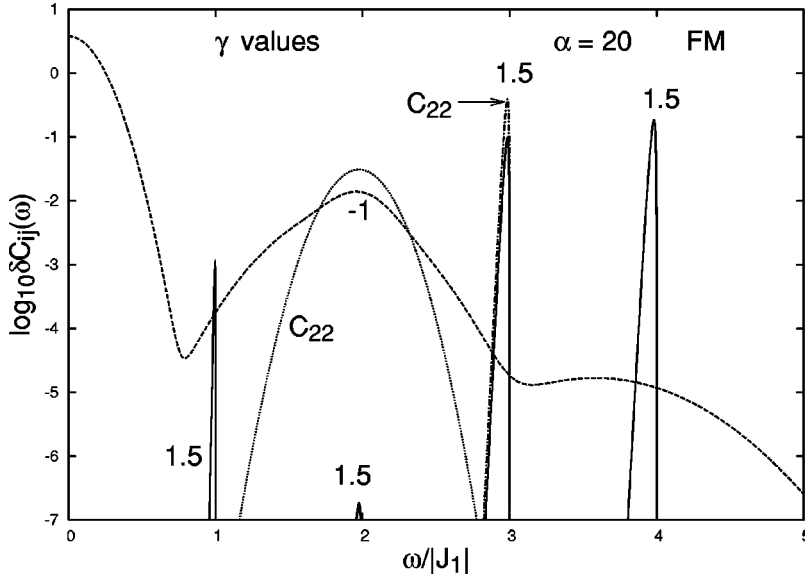


FIG. 12. Plots at $\alpha=20$ of the FM $\log_{10}[\delta\tilde{C}_{11}(\omega)]$ for $\gamma=1.5$ (solid) and -1 (dashed) and $\log_{10}[\delta\tilde{C}_{22}(\omega)]$ for $\gamma=1.5$ (dot-dashed) and -1 (dotted) vs $\omega/|J_1|$.

$$\begin{aligned} \Omega_2(\gamma)/J_1 &= 0 \quad \text{for } \gamma \leq -1/2, \\ &= 1 + 2\gamma \quad \text{for } \gamma \geq -1/2, \end{aligned} \quad (33)$$

$$\begin{aligned} \Omega_3(\gamma)/J_1 &= 2|1 - 1/\gamma| \quad \text{for } \gamma < -1/2, \\ &= |5 - 2\gamma| \quad \text{for } \gamma \geq -1/2, \end{aligned} \quad (34)$$

$$\begin{aligned} \Omega_4(\gamma)/J_1 &= |1 - 1/\gamma| \quad \text{for } \gamma \leq -1/2, \\ &= 2|1 - \gamma| \quad \text{for } \gamma \geq -1/2. \end{aligned} \quad (35)$$

As for the AFM case with $1 \neq \gamma > 1/2$, for $\gamma < -1/2$, the low- T FM mode with frequency $\Omega_2(\gamma)=0$ is a central peak, and Ω_1 and Ω_4 are finite and degenerate. For $\gamma > -1/2$, there are four FM magnon modes, none of which is a central peak. The amplitude of the weakest mode with frequency $\Omega_3(\gamma)$ is $\propto T^2$ as $T \rightarrow 0$ for $\gamma \geq -1/2$. At $\gamma=5/2$, $\Omega_3(5/2) \propto T$, so the mode with frequency $\Omega_3(\gamma)$ is never a central peak.

For the low- T FM equilateral triangle, indicated by the circle in Fig. 13, $\delta\tilde{C}_{22}(\omega) = \delta\tilde{C}_{11}(\omega)$, since the amplitude of the mode with frequency $\Omega_4(\gamma)$ vanishes as $\gamma \rightarrow 1$, and the remaining mode frequencies are degenerate. Hence $\delta\tilde{C}_{11}(\omega)$ approaches the FM scaling form shown in Fig. 6.

We now examine the other special FM case $\gamma = -1/2$. The mode $\Omega_2(-1/2)$, indicated by the triangle in Fig. 13, is a low- T FM mode with scaling properties remarkably similar to those of the AFM mode with frequency $\Omega_2(1/2)$, pictured in Fig. 10. As $T \rightarrow 0$, the $\delta\tilde{C}_{11}(\omega)$ FM mode frequency $\Omega_2(-1/2) \rightarrow |J_2|/|\alpha|^{1/2}$, and the mode shape approaches a scaling function of $|\alpha|^{1/2}\omega/|J_1|$, as pictured in Fig. 14. By comparing Fig. 14 with Fig. 11, the lowest T curves in the two figures are almost identical, provided that one rescales T by a factor of 8. Since in these special cases, the scaling does not involve scaling of the mode amplitude, it does not represent a contribution to $\delta\mathcal{C}_{11}(t)$ involving a scaling of the time, as for the AFM equilateral triangle pictured in Fig. 5, or more generally for the AFM low- T equivalent neighbor and four-

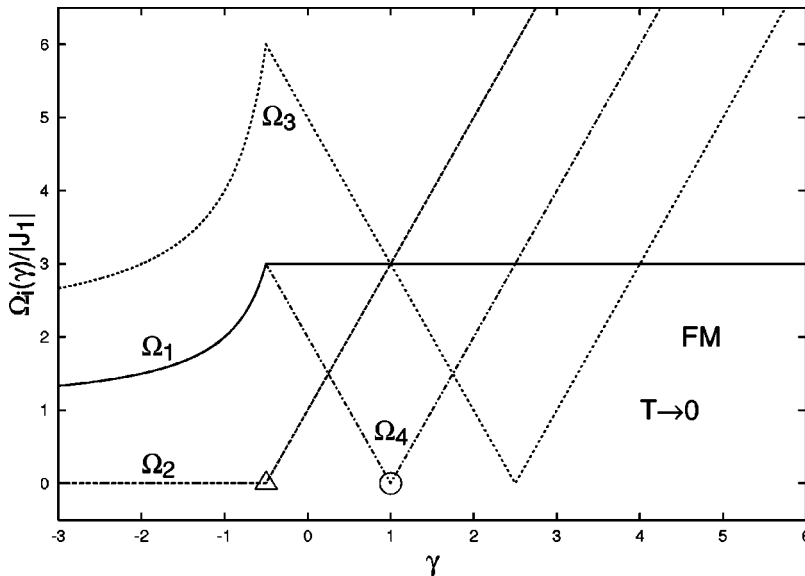


FIG. 13. Plots of the low- T FM mode frequencies Ω_i/J_1 vs γ . The triangle indicates low- T mode scaling, and the circle indicates the disappearance of the mode. See the text.

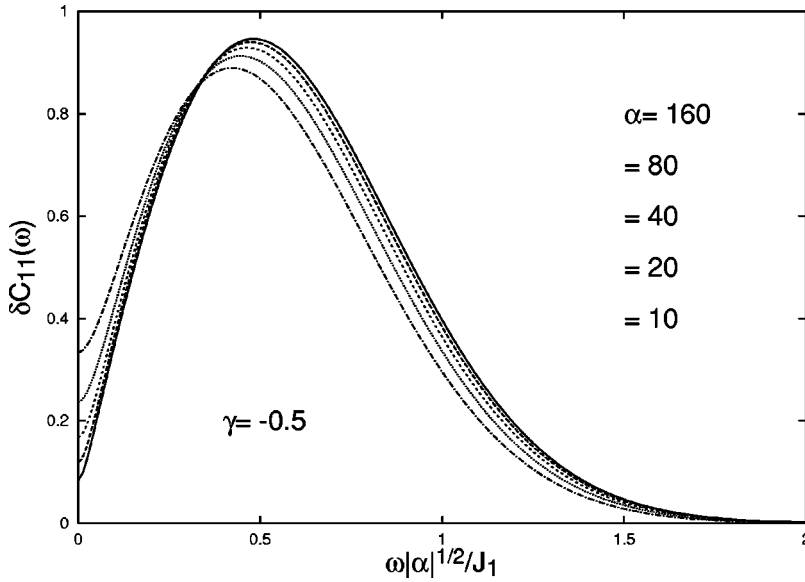


FIG. 14. Plots at various low T values of $\delta\tilde{C}_{11}(\omega)$ vs the scaled frequency $\omega|\alpha|^{1/2}/J_1$ for the FM $\Omega_2(-0.5)$ mode.

spin ring models.^{21,22} It is therefore a new form of mode scaling, not previously found in any SMM system.

V. SUMMARY AND DISCUSSION

We presented the exact solution for the thermal equilibrium dynamics of three classical Heisenberg spins on a triangle with two exchange couplings J_1 and J_2 . Although one might expect that for $\gamma = J_2/J_1 \approx 1$ the behavior would not be too different from that of the equilateral triangle, $\gamma = 1$, we found that this is not the case, regardless of T . Instead of the two $\mathcal{C}_{ij}(t)$'s related by a sum rule for $\gamma = 1$, for $\gamma \neq 1$ there are four $\mathcal{C}_{ij}(t)$'s related by a sum rule. For $\gamma \neq 0$, the piecewise continuous Fourier transforms $\delta\tilde{C}_{ij}(\omega)$ demonstrate the profound effects of the absence of translational symmetry within the triangle with $\gamma \neq 1$. As $T \rightarrow \infty$, they allow us to determine the long-time behavior of the autocorrelation functions $\mathcal{C}_{11}(t)$ and $\mathcal{C}_{22}(t)$, which approach their distinct long-time asymptotic limits differently, as t^{-2} and t^{-3} , respectively. For the three-spin chain, $\gamma = 0$, the autocorrelation function on the chain end, $\delta\tilde{C}_{11}(\omega)$, is discontinuous at $\omega/|J_1| = 1$ at all T , leading to the characteristic t^{-1} behavior of $\mathcal{C}_{11}(t)$ as $T \rightarrow \infty$.

At low T , setting $\gamma \neq 1$ leads to a qualitatively different behavior from that obtained for $\gamma = 1$. Regardless of the sign of J_1 , for $\gamma \neq 1$, there are four low- T modes in $\delta\tilde{C}_{11}(\omega)$. For $J_1 < 0$ and $\gamma \neq 1$, two of these low- T modes, Ω_1 and Ω_4 , are degenerate for $\gamma \geq 1/2$. For $J_1 > 0$, Ω_1 and Ω_4 are degenerate for $\gamma \leq -1/2$. In both of these FM and AFM regimes, one of the nondegenerate low- T modes is a central peak with a width determined by the J_i , which grows in intensity as $T \rightarrow 0$. This central peak, which can have the largest mode intensity, arises from the pinning of a magnon mode in the isosceles triangle with $J_1 \neq J_2$, and does not appear in any other model which has been solved exactly. There is also a peak at $\omega = 0$ arising from the long-time asymptotic limit of $\mathcal{C}_{11}(t)$, which would be broadened by relaxation processes not included in our model.

For the three-spin chain, $\gamma = 0$, the effects of the absence of translational symmetry in the chain are even more dramatic, leading to qualitatively different dynamical behaviors of the spins on the chain ends from that of the spin at the center. For both signs of J_1 , $\delta\tilde{C}_{22}(\omega)$ has only one mode energy $|J_1|$. But $\delta\tilde{C}_{11}(\omega)$ is distinctly different. For the AFM three-spin chain, $\delta\tilde{C}_{11}(\omega)$ has three low- T modes at $n|J_1|$ with $n = 1, 2, 3$, where the $n = 1$ mode is doubly degenerate. For the FM three-spin chain, $\delta\tilde{C}_{11}(\omega)$ has four modes at $n|J_1|$ with $n = 1, 2, 3$, and 5. Our results suggest that for N -spin chains, the spins on or near the chain ends would have a richer dynamics than would those of more central spins, or of spins on closed rings of N spins. It would be interesting to see if such differences are indeed maintained for larger spin chains and for larger spin clusters with two or more Heisenberg spin exchange interactions.

For the four-spin ring with equal near-neighbor exchange couplings J_1 , the single autocorrelation function $\delta\tilde{C}_{11}(\omega)$ has a single mode that approaches the fixed frequency $2|J_1|$ as $T \rightarrow 0$, in addition to the AFM (FM) mode of the four-spin equivalent neighbor model with a frequency that approaches 0 ($4|J_1|$).^{21,22} None of these is a central peak at $T \neq 0$. The isosceles triangle has a much richer spectrum of four modes, with tunable frequencies that depend upon γ , and a central peak for a semi-infinite range of γ values. In addition, at the onset of the central peak, that mode form exhibits low- T frequency scaling, instead of the time scaling present in the AFM equivalent neighbor and four-spin ring models, and it is a scaling function of a differently scaled frequency than in the FM equivalent neighbor model and the four-spin ring.^{21,22} The simplest integrable four-spin system with dynamics similar to that of the isosceles triangle is the squashed tetrahedron, which also involves two different near-neighbor exchange couplings.²⁵

Inelastic neutron scattering experiments on large single crystals would be a particularly useful technique to observe the effects predicted here. By appropriately varying the scat-

tering wave vector, all four of the $\delta\tilde{\mathcal{C}}_{ij}(\omega)$'s can be measured as functions of ω and T . Although experimental observation of the predicted low- T modes might be difficult, since quantum effects are expected to dominate at very low T , the presence of such modes for three classical Heisenberg spins on an isosceles triangle underscores the qualitative changes that occur with different exchange couplings. Our numerical results indicate that the development of these additional modes appears at T values high enough for the classical treatment to be valid.

ACKNOWLEDGMENTS

The authors thank P. Khalifah, K. Morawetz, S. E. Nagler, K. Scharnberg, and D. Sen for helpful discussions.

APPENDIX

We first discuss the $T \rightarrow \infty$ limit of the integrals $I_i(t)$, Eqs. (16)–(18). From Eq. (13), we obtain $\delta\mathcal{C}_{22}(t) = I_1(t)/4$. As $T \rightarrow \infty$, $\delta\mathcal{C}_{22}(t)$ coincides with that of the $N=3$ equivalent neighbor model, so $\lim_{T \rightarrow \infty} I_1(t)$ is obtained by setting $N=3$ in Eqs. (4)–(9) of Ref. 22. Setting $t^* = J_1 t$ as before, for $I_2(t)$ we find

$$\lim_{T \rightarrow \infty} I_2(t) = \int_0^2 dx f_2(x) \cos[(1-\gamma)xt^*], \quad (\text{A1})$$

$$f_2(x) = \frac{4-x^2}{256x^2} \left[4x(x^2+1) - (x^2-1)^2 \ln \left(\frac{x+1}{x-1} \right) \right]. \quad (\text{A2})$$

Then Eq. (23) is derived from $f_2(0) = f_2(2) = 0$, and

$$f_2'(0) = \frac{1}{6}, \quad f_2'(2) = -\frac{5}{32} + \frac{9}{128} \ln 3. \quad (\text{A3})$$

Since $f_2(x)$ and $f_2'(x)$ are continuous at $x=1$, Eq. (A3) leads to the constants a_1 and a_2 in Eq. (23). The FT of $I_3(t)$ at arbitrary T is given in Eqs. (A10)–(A13).

We illustrate the procedure for computing the FT's by obtaining $\delta\tilde{\mathcal{C}}_{22}(\omega)$. The FT of $\cos(st^*)$ is $\delta(\tilde{\omega}+s) + \delta(\tilde{\omega}-s)$, where $\tilde{\omega} = \omega/J_1$. For a $\tilde{\omega} > 0$, the $\delta(\tilde{\omega}+s)$ term is irrelevant. Then $\tilde{\omega}$ satisfies $|x-1| \leq \tilde{\omega} \leq x+1$. For fixed $\tilde{\omega}$, the integration interval for x is then determined as a function of $\tilde{\omega}$. Hence

$$\delta\tilde{\mathcal{C}}_{22}(\omega) = \frac{1}{4Z} \Theta(3-\tilde{\omega}) \int_{|\tilde{\omega}-1|}^{\min[2,(\tilde{\omega}+1)]} dx \mathcal{F}_{22}(x), \quad (\text{A4})$$

$$\mathcal{F}_{22}(x) = e^{\alpha[\tilde{\omega}^2 + (\gamma-1)x^2]} \tilde{\omega} \left[1 - \left(\frac{\tilde{\omega}^2 + 1 - x^2}{2\tilde{\omega}} \right)^2 \right], \quad (\text{A5})$$

and $\Theta(z)$ is Heaviside's step function, $\Theta(z) = 0$ if $z < 0$, $\Theta(z) = 1$ if $z > 0$.

The exact calculation of $\delta\tilde{\mathcal{C}}_{11}$ is substantially more involved. We define the functions $\tilde{I}_a(\omega)$ to be FT's of $I_a(t)$, [Eqs. (16)–(18)],

$$\delta\tilde{\mathcal{C}}_{11}(\omega) = \tilde{I}_1(\omega) + \tilde{I}_2(\omega) + \tilde{I}_3(\omega), \quad (\text{A6})$$

where $\tilde{I}_1(\omega) = \delta\tilde{\mathcal{C}}_{22}(\omega)/4$. We then find that

$$\tilde{I}_2(\omega) = \frac{1}{2Z|1-\gamma|} \Theta(2-\tilde{\omega}) \int_{|1-\tilde{\omega}|}^{1+\tilde{\omega}} ds \mathcal{F}_{11,2}(s), \quad (\text{A7})$$

$$\mathcal{F}_{11,2}(s) = e^{\alpha[s^2 + (\gamma-1)\tilde{\omega}^2]} s \left[1 - \frac{\tilde{\omega}^2}{4} \right] \left[1 - \left(\frac{s^2 + \tilde{\omega}^2 - 1}{2s\tilde{\omega}} \right)^2 \right], \quad (\text{A8})$$

and $\tilde{\omega} = \omega/[J_1(1-\gamma)]$. We first write $\tilde{I}_3(\omega)$ as

$$\tilde{I}_3(\omega) = \frac{1}{16Z} [\tilde{I}_{3a}(\tilde{\omega}) + \tilde{I}_{3b}(\tilde{\omega}) + \tilde{I}_{3c}(\tilde{\omega})]. \quad (\text{A9})$$

For $0 < \gamma < 2$, setting $\Delta = |1-\gamma|$, we then have

$$\begin{aligned} \tilde{I}_{3a}(\tilde{\omega}) &= \Theta(3+2\Delta-\tilde{\omega}) \Theta(\tilde{\omega}-1) \\ &\times \int_{(\tilde{\omega}-1)/(1+\Delta)}^{\min[2,(\tilde{\omega}+1)/(1+\Delta)]} dx \mathcal{F}_{11,3-}(x) \\ &+ \Theta(1-\tilde{\omega}) \Theta(\tilde{\omega}-\Delta) \int_{(1-\tilde{\omega})/(1-\Delta)}^{(1+\tilde{\omega})/(1+\Delta)} dx \mathcal{F}_{11,3-}(x), \end{aligned} \quad (\text{A10})$$

$$\begin{aligned} \tilde{I}_{3b}(\tilde{\omega}) &= \Theta(3-2\Delta-\tilde{\omega}) \Theta(\tilde{\omega}-1) \\ &\times \int_{(\tilde{\omega}-1)/(1-\Delta)}^2 dx \mathcal{F}_{11,3+}(x) + \Theta(1-\tilde{\omega}) \\ &\times \int_{(1-\tilde{\omega})/(1+\Delta)}^{\min[2,(1+\tilde{\omega})/(1-\Delta)]} dx \mathcal{F}_{11,3+}(x), \end{aligned} \quad (\text{A11})$$

$$\tilde{I}_{3c}(\tilde{\omega}) = \Theta(\Delta-\tilde{\omega}) \int_{(1+\tilde{\omega})/(1+\Delta)}^{\min[2,(1-\tilde{\omega})/(1-\Delta)]} dx [-\mathcal{F}_{11,3-}(x)], \quad (\text{A12})$$

$$\begin{aligned} \mathcal{F}_{11,3\pm}(x) &= e^{\alpha[(\tilde{\omega} \pm x\Delta)^2 + (\gamma-1)x^2]} \\ &\times \frac{(1-x^2/4)[(\tilde{\omega} \pm x(1+\Delta))^2 - 1]^2}{(\tilde{\omega} \pm x\Delta)x^2}. \end{aligned} \quad (\text{A13})$$

For other values of γ , we obtain similar expressions.

As $T \rightarrow \infty$, one has

$$\lim_{T \rightarrow \infty} \tilde{I}_2(\omega) = \frac{1}{|1-\gamma|} \Theta(2-\tilde{\omega}) f_2(\tilde{\omega}). \quad (\text{A14})$$

The general expression for $\lim_{T \rightarrow \infty} \tilde{I}_3(\omega)$ is too complicated to be given here. For the chain,

$$\begin{aligned} \lim_{T \rightarrow \infty} \tilde{I}_3^{\gamma=0}(\omega) &= \Theta(5 - \tilde{\omega})\Theta(\tilde{\omega} - 3) \frac{1}{64} \tilde{I}_{3a}^{\gamma=0}(\tilde{\omega}) \\ &+ \Theta(3 - \tilde{\omega})\Theta(\tilde{\omega} - 1) \frac{1}{64} \tilde{I}_{3b}^{\gamma=0}(\tilde{\omega}) \\ &+ \Theta(1 - \tilde{\omega}) \frac{1}{64} \tilde{I}_{3c}^{\gamma=0}(\tilde{\omega}), \end{aligned} \quad (\text{A15})$$

$$\begin{aligned} \tilde{I}_{3a}^{\gamma=0}(\tilde{\omega}) &= \frac{(5 - \tilde{\omega})(-24 - 195\tilde{\omega} + 229\tilde{\omega}^2 + 47\tilde{\omega}^3 + 7\tilde{\omega}^4)}{48\tilde{\omega}} \\ &+ \frac{(\tilde{\omega}^2 - 1)(1 + 7\tilde{\omega}^2)}{\tilde{\omega}^2} \ln \frac{\tilde{\omega} - 1}{4} \\ &- \frac{(\tilde{\omega}^2 - 4)(\tilde{\omega}^2 - 1)^2}{4\tilde{\omega}^2} \ln \frac{\tilde{\omega} + 1}{2(\tilde{\omega} - 2)}, \end{aligned} \quad (\text{A16})$$

$$\begin{aligned} \tilde{I}_{3b}^{\gamma=0}(\tilde{\omega}) &= \frac{3\tilde{\omega}^4 + 67\tilde{\omega}^2 - 24}{6\tilde{\omega}} \\ &- \frac{(\tilde{\omega}^2 - 1)(\tilde{\omega}^4 + 23\tilde{\omega}^2 + 8)}{4\tilde{\omega}^2} \ln \frac{\tilde{\omega} + 1}{\tilde{\omega} - 1}, \end{aligned} \quad (\text{A17})$$

$$\begin{aligned} \tilde{I}_{3c}^{\gamma=0}(\tilde{\omega}) &= \frac{7\tilde{\omega}^4 - 6\tilde{\omega}^2 + 951}{24} + \frac{(1 - \tilde{\omega}^2)(1 + 7\tilde{\omega}^2)}{\tilde{\omega}^2} \ln \frac{1 - \tilde{\omega}^2}{16} \\ &+ \frac{(4 - \tilde{\omega}^2)(1 - \tilde{\omega}^2)^2}{4\tilde{\omega}^2} \ln \frac{4(4 - \tilde{\omega}^2)}{1 - \tilde{\omega}^2}. \end{aligned} \quad (\text{A18})$$

The leading asymptotic behavior [Eq. (22)], arises from

$$\tilde{I}_{3a}^{\gamma=0}(5) = 0, \quad (\text{A19})$$

$$\tilde{I}_{3a}^{\gamma=0}(3) = \tilde{I}_{3b}^{\gamma=0}(3) = \frac{137}{3} - \frac{592}{9} \ln 2, \quad (\text{A20})$$

$$\tilde{I}_{3b}^{\gamma=0}(1) = \frac{23}{3}, \quad \tilde{I}_{3c}^{\gamma=0}(1) = \frac{119}{3}, \quad (\text{A21})$$

$$\tilde{I}_{3c}^{\gamma=0}(0) = \frac{315}{8} - 33 \ln 2. \quad (\text{A22})$$

We now derive the AFM low- T mode frequency $\Omega_2(\gamma)$. As $\alpha \rightarrow -\infty$, the integrand in Eq. (A4) becomes sharply peaked about some ω -dependent value x_0 . We then perform an asymptotic evaluation of the form

$$\int_a^b dx e^{h(x)} \approx e^{h(x_0)} \sqrt{2\pi \left| \frac{d^2 h}{dx^2} \right|_{x_0}^{-1}}, \quad (\text{A23})$$

$$h(x) = \alpha [\tilde{\omega}^2 + (\gamma - 1)x^2] + \ln \tilde{\omega} + \ln \left[1 - \frac{(1 + \tilde{\omega}^2 - x^2)^2}{4\tilde{\omega}^2} \right]. \quad (\text{A24})$$

Inside the integration region, the integrand has exactly one maximum at x_0 . For $\gamma > 1$, $x_0^{(\gamma > 1)} = |1 - \omega| + \epsilon$, while for $\gamma < 1$, $x_0^{(\gamma < 1)} = 1 + \omega - \epsilon$, where $\epsilon > 0$ is $\mathcal{O}(\alpha^{-1})$. We then evaluate the integral in Eq. (A23). It is maximal for $\omega = \Omega_1$, where

$$\Omega_1(\gamma)/|J_1| = |1 - 1/\gamma|. \quad (\text{A25})$$

For $\gamma < 1/2$, this result gives a spurious maximum, since it would require $x > 2$. Since the result of the asymptotic evaluation is a monotonically increasing function of ω for $\omega < 1$, we therefore conclude that $\Omega_1 = |J_1|$ for $\gamma < 1/2$. The proof of Eq. (28) is thus complete.

- ¹R. Sessoli, D. Gatteschi, A. Caneschi, and M. A. Novak, *Nature (London)* **365**, 141 (1993).
- ²D. Gatteschi, A. Caneschi, L. Pardi, and R. Sessoli, *Science* **265**, 1054 (1994).
- ³D. Gatteschi, *Adv. Mater.* **6**, 634 (1994).
- ⁴*Magnetic Molecular Materials*, Vol. 198 of *NATO Advanced Studies Series E: Applied Sciences*, edited by D. Gatteschi, O. Kahn, J. S. Miller, and F. Palacio (Kluwer Academic, Norwell, MA, 1991).
- ⁵J. R. Friedman, M. P. Sarachik, J. Tejada, and R. Ziolo, *Phys. Rev. Lett.* **76**, 3830 (1996).
- ⁶L. Thomas, F. Lonti, R. Allou, D. Gatteschi, R. Sessoli, and B. Barbara, *Nature (London)* **383**, 145 (1996).
- ⁷D. Gatteschi, *J. Alloys Compd.* **317**, 8 (2001).
- ⁸M. N. Leuenberger and D. Loss, *Nature (London)* **410**, 789 (2001).
- ⁹Y. Furukawa, A. Iwai, K. I. Kumagai, and A. Yakubovsky, *J.*

- Phys. Soc. Jpn.* **65**, 2393 (1996).
- ¹⁰A. Lascialfari, F. Tabak, G. L. Abbati, F. Borsa, M. Corti, and D. Gatteschi, *J. Appl. Phys.* **85**, 4539 (1999).
- ¹¹A. Müller, J. Meyer, H. Bögge, A. Stammli, and A. Botar, *Chem.-Eur. J.* **4**, 1388 (1998).
- ¹²J.-P. Costes, F. Dahan, and F. Nicodème, *Inorg. Chem.* **40**, 5285 (2001).
- ¹³J. T. Rijssenbeek, R. Jin, Yu. Zadorozhny, Y. Liu, B. Batlogg, and R. J. Cava, *Phys. Rev. B* **59**, 4561 (1999).
- ¹⁴P. Khalifah, Ph.D. thesis, Princeton University, 2001.
- ¹⁵D. Mentrup, J. Schnack, and M. Luban, *Physica A* **272**, 153 (1999).
- ¹⁶D. V. Efremov and R. A. Klemm, *Phys. Rev. B* **66**, 174427 (2002).
- ¹⁷D. Mentrup, H. J. Schmidt, J. Schnack, and M. Luban, *Physica A* **278**, 214 (2000).
- ¹⁸N. Srivastava, C. Kaufman, and G. Müller, *J. Appl. Phys.* **63**, 4154 (1988).

¹⁹G. Müller, J. Phys. (Paris), Colloq. **49**, C8-1403 (1988).

²⁰M. Luban and J. H. Luscombe, Am. J. Phys. **67**, 1161 (1999).

²¹R. A. Klemm and M. Luban, Phys. Rev. B **64**, 104424 (2001).

²²R. A. Klemm and M. Ameduri, Phys. Rev. B **66**, 012403 (2002).

²³This is known as the first Riemann-Lebesgue lemma.

²⁴Our definition of δ_3 agrees with that in Ref. 22, but differs by a factor of 2 from that in Refs. 20 and 21.

²⁵M. Ameduri and R. A. Klemm (unpublished).